Published by Nigerian Society of Physical Sciences. Hosted by FLAYOO Publishing House LTD

Proceedings of the Nigerian Society of Physical Sciences

Journal Homepage: https://flayoophl.com/journals/index.php/pnspsc

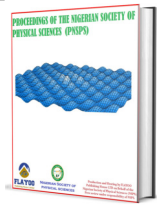

Stacking ensemble machine learning for predicting land surface temperature hotspots using landsat 9 data

Momohjimoh Abdulsalami[a,*], Joseph Omeiza Alao[b], Zainab Usman[c], Bunmi Oyekola Isaac[c], Danga Onimisi Abdulmalik[c], Michael Adewale Ibitomi[d], Yahaya Jibrin Danjuma[e], Saratu Muhammad Hussaini[b], Dahiru Dahuwa[f], Aliyu Abdullateef[c]

[a]*Department of Physics, Confluence University of Science and Technology, Osara*
[b]*Department of Physics, Air Force Institute of Technology, Kaduna*
[c]*Department of Geosciences, Confluence University of Science and Technology, Osara*
[d]*Department of Mineral and Petroleum Resources Engineering, Kogi State Polytechnic, Lokoja*
[e]*Department of Mathematics and Statistics, Confluence University of Science and Technology, Osara*
[f]*Department of Physics, Federal university of Health sciences, Azare*

ABSTRACT

Despite advancements in predictive modeling, existing methods struggle with accuracy and spatial variability in Land Surface Temperature (LST) estimation. This study presents a Stacking Ensemble Model (SEM) integrating Random Forest (RF), eXtreme Gradient Boosting (XGBoost), and k-Nearest Neighbors (KNN) to enhance LST prediction using Landsat 9 and SRTM DEM data in Kogi State, Nigeria. The SEM outperformed individual models, achieving an R^2 of 99.86%, surpassing RF by 3.31%, XGBoost by 8.03%, and KNN by 12.79%. Results revealed significant spatial variability, with temperatures ranging from 24.8°C to 49.3°C and critical hotspots above 40°C covering 1,035 km^2, supporting geothermal energy exploration. Incorporating elevation spectral indices and key predictors like NDVI, proportion of vegetation, land surface emissivity, and brightness temperature further improved accuracy. This SEM framework enhances predictive robustness, scalability, and spatial analysis for better LST modeling.

Keywords: LST, Geothermal energy, Machine learning, Landsat 9.

DOI:10.61298/pnspsc.2025.2.158

1. INTRODUCTION

Surface Temperature (Ts), often called Land Surface Temperature (LST), reflects land-atmosphere interactions and energy transfer processes within the Earth's interior. Understanding LST is crucial for assessing heat flux, which is influenced by thermal conductivity and land cover properties. High thermal conductivity materials, such as bare rock and urban surfaces, facilitate rapid heat transfer, leading to localized temperature increases, whereas vegetative and water-covered areas moderate temperature fluctuations by acting as thermal insulators [1, 2]. Despite advancements in satellite technologies such as Landsat 9 and SRTM DEM, challenges persist, including atmospheric interference, spatial resolution limitations, and land-use dynamics, necessitating innovative predictive frameworks for improved ac-

*Corresponding Author Tel. No.: +234-816-7577-770.
e-mail: abdulsalamim@custech.edu.ng (Momohjimoh Abdulsalami)

curacy [3].

Studies have used datasets like Landsat and MODIS for surface temperature estimations, emphasizing their respective strengths. MODIS, with its high temporal resolution (daily revisit), effectively captures temperature dynamics over time but has coarse spatial resolution (1 km), limiting fine-scale analysis. In contrast, Landsat 9 offers high spatial resolution (30 m for reflective bands and 100 m for thermal bands), allowing for detailed temperature mapping, though with a lower temporal resolution (16-day revisit cycle) [4]. Researchers have integrated MODIS and Landsat data to balance spatial and temporal trade-offs [5–7]. Studies in Nigeria [6, 8] highlight the effectiveness of Landsat data in analyzing urban heat islands and LST variations caused by urbanization.

Landsat 9 and SRTM DEM, with their improved spatial and spectral capabilities, provide new opportunities for precise surface temperature estimation. However, as noted by [4, 9], their full potential in geothermal energy exploration remains underutilized. Integrating high-resolution remote sensing data with advanced machine learning models, particularly stacking ensemble methods, can enhance predictive accuracy and detect thermal anomalies.

Machine learning approaches, especially ensemble models, have significantly improved the accuracy of surface temperature predictions by capturing complex spatial and temporal interactions within environmental datasets. Studies employing machine learning algorithms, such as Random Forest (RF), Artificial Neural Networks (ANN), and Adaptive Neuro-Fuzzy Inference Systems (ANFIS), have demonstrated remarkable accuracy in predicting surface temperature [9–14] applied an Adaptive Neuro-Fuzzy Inference System (ANFIS) to predict surface temperature with remarkable precision (R^2 = 0.99). Ref. [14] demonstrated the efficacy of stacking ensemble models by combining tree-based algorithms such as LightGBM and XGBoost with deep learning architectures like Convolutional Neural Networks (CNN). Studies by [9, 12] have further underscored the potential of Random Forest (RF) and Artificial Neural Networks (ANN) in surface temperature prediction, highlighting their scalability and superior accuracy compared to traditional approaches.

Ensemble machine learning techniques, particularly stacking models, have shown great promise in addressing the complexities of remotely sensed data prediction by integrating multiple algorithms to harness their strengths. While single models such as Random Forest [9], K-Nearest Neighbors (KNN) [14], and ANN [10, 12] offer valuable insights, they often struggle to capture the full extent of spatial variability, nonlinear interactions, and diverse environmental factors in surface temperature data. In contrast, stacking ensemble models, such as the framework proposed by Ref. [14], combine multiple machines learning techniques, including LightGBM, XGBoost, and CNN, to improve accuracy and robustness, particularly in high-dimensional datasets. However, the application of these ensemble methods to surface temperature modeling remains limited, with significant challenges related to computational demands and the integration of high-resolution remote sensing data [3, 13]

By combining outputs from RF, KNN, and XGBoost, stacking ensembles enhance predictive accuracy, robustness, and generalization, addressing the limitations of individual models. This

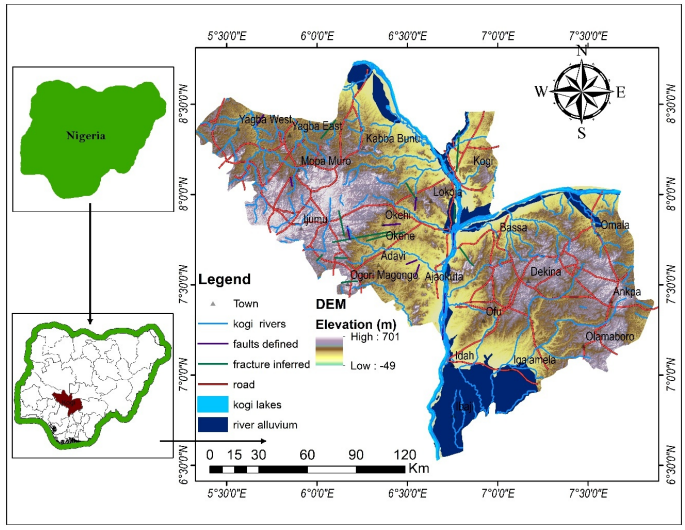

Figure 1. Location map of the study area.

aligns with the principle that no single machine-learning model is optimal for all scenarios [15], making stacking ensembles a powerful and adaptable tool for improving LST prediction.

Numerous studies have examined surface temperature dynamics within urban and semi-urban settings, offering valuable insights into the factors influencing temperature variations. Ref. [16] documented significant surface temperature variations of up to 10.9°C between urban and rural areas in Lokoja, driven by vegetation loss and urban expansion. Similarly, Ref. [6] observed a 4.91°C increase over 24 years in Akure, attributing the rise to rapid urbanization. In Port Harcourt, Ref. [17] reported seasonal surface temperature differences of 9.3°C during the rainy season and 4.8°C in the dry season, highlighting the influence of vegetation and land-use dynamics on surface temperature in urban environments. These investigations underscore the complex interplay between urbanization and thermal environments, emphasizing the importance of sustainable urban planning to manage surface temperature effectively.

This study seeks to address existing gaps by developing a robust and scalable stacking ensemble model for surface temperature prediction using spectral data of Landsat 9 and SRTM DEM data. The proposed model integrates diverse environmental variables to enhance predictive accuracy and identify thermal anomalies, including potential sites for geothermal energy exploration. According to Ref. [18], surface temperatures as low as 40°C are considered indicative of geothermal potential; however, they caution that surface temperature alone is insufficient for accurately assessing geothermal viability. By addressing these methodological gaps, this study aims to make substantial contributions to the fields of renewable energy exploration and environmental monitoring.

1.1. STUDY AREA

This study was conducted in Kogi State, Nigeria, encompassing an area of approximately 29,833 km^2. The state is geographically situated between latitudes 6°30′-8°50′N and longitudes 5°30′–7°50′E, as illustrated in Figure 1.

Kogi State is renowned for the confluence of the Niger and

Benue Rivers at Lokoja, its capital. The region's varied elevation, ranging from -49 m to 701 m above sea level, supports a wide range of activities, including agriculture, urban development, geothermal energy exploration, and mining, all of which significantly influence Surface Temperature.

The mapped hydrological features, such as rivers, lakes, alluvium and fractures, underscore the region's potential for geothermal activity. This research provides critical insights into the sustainable exploration of geothermal energy resources in Kogi State.

2. MATERIALS AND METHODS

2.1. DATA SOURCE

The primary dataset for Land Surface Temperature (LST) analysis was obtained from Landsat 9 Tier 1 Surface Reflectance, accessed via Google Earth Engine (GEE). Landsat 9, a joint mission by NASA and USGS, provides 30 m spatial resolution for reflective bands and 100 m for Thermal Infrared (TIR) bands. The dataset is pre-processed to correct for radiometric and geometric distortions, ensuring high-quality temporal and spatial analysis of surface properties.

2.2. SHUTTLE RADAR TOPOGRAPHY MISSION (SRTM) DEM AND LANDSAT 9

The SRTM DEM, acquired by NASA's Jet Propulsion Laboratory (JPL), provides 30 m resolution elevation data, accessible via GEE [19]. In this study, SRTM DEM was used alongside Landsat 9 spectral data to predict surface temperature across 21 major towns in Kogi State. Elevation spectral indices quantify topographic variations using Digital Elevation Models (DEMs). These indices influence LST prediction by affecting surface energy balance, airflow dynamics, and solar radiation distribution, making them essential for accurate temperature modeling.

Landsat 9 and SRTM DEM were selected due to their high spatial resolution, reliable temporal coverage, and suitability for LST prediction and topographic analysis. Landsat 9 offers 30 m multispectral and 100 m thermal resolution, significantly finer than MODIS (1 km thermal resolution), enabling detailed LST mapping [20]. Its 16-day revisit cycle ensures consistent monitoring, unlike ASTER, which, despite its five thermal bands at 90 m resolution, has limited global coverage and inconsistent availability. Additionally, SRTM DEM's 30 m resolution provides better topographic representation than the freely available ASTER 90 m DEM [19]. Landsat 9 and SRTM DEM are freely accessible via USGS and GEE, making them ideal for cost-effective and reproducible studies. Their integration enhances LST estimation by incorporating elevation-driven temperature variations, further justifying their selection over MODIS and ASTER.

2.3. ANALYTIC PLATFORM

The data were processed and analyzed using the following platforms:

i. Google Earth Engine (GEE): Used for pre-processing and performing spatial computations on satellite imagery.
ii. Google Colab: Utilized for implementing machine learning algorithms in a cloud-based Python environment.
iii. ArcGIS: Applied for map scaling.

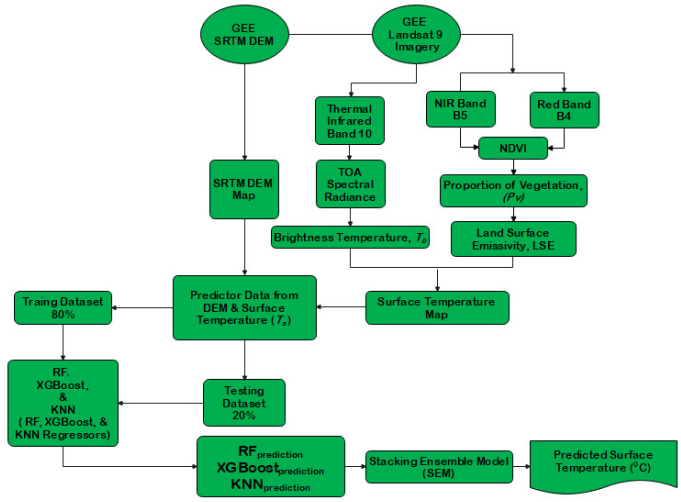

Figure 2. Flow chart of the study.

2.4. DATA PREPROCESSING

The Land Surface Temperature (LST) estimation (Figure 2) was conducted using Landsat 9 Tier 1 Surface Reflectance data in Google Earth Engine (GEE). The Landsat 9 images were filtered based on the Region of Interest (ROI), cloud cover (<1%), and date range (January 2022 – June 2024). A median composite of the selected images was created and clipped to the study area to minimize cloud interference. Brightness Temperature (BT) was derived from the Thermal Infrared (TIR) Band 10 using thermal conversion coefficients. The Normalized Difference Vegetation Index (NDVI) was then computed from the Near-Infrared (Band 5) and Red (Band 4) bands. Land Surface Emissivity (E) was estimated from NDVI values, and the Planck function was applied to convert BT into LST in Kelvin, which was subsequently converted to degrees Celsius.

Additionally, the Shuttle Radar Topography Mission (SRTM) Digital Elevation Model (DEM) was downloaded and processed to generate an elevation map of the study area. The DEM was integrated with LST-derived variables, including Brightness Temperature, Emissivity, Proportion of Vegetation, and NDVI, to enhance LST prediction accuracy. The classified LST maps were then exported, and the total area covered by each temperature category was calculated in square kilometers using pixel-based area computations. This approach leverages the high spatial resolution of Landsat 9 and the topographic influence of SRTM DEM to improve LST estimation, providing a robust methodology for surface temperature analysis in the study area.

2.5. RADIOMETRIC CALIBRATION TO TOP OF ATMOSPHERE (TOA) RADIANCE

Landsat 9 Tier 1 Surface Reflectance data include Top of Atmosphere (TOA) radiance correction using the Land Surface Reflectance Code (LaSRC) algorithm, which removes aerosol and Rayleigh scattering effects [21]. The thermal band 10 undergoes atmospheric correction, ensuring accurate Land Surface Temperature (LST) retrieval without additional adjustments. The DN-to-radiance conversion follows this equation:

$$A_\lambda = L_m \, x \, DN + R_A, \quad (1)$$

where A_λ is the TOA radiance in watts per square meter per steradian per micrometer $\left(W/m^2 sr\ \mu m\right)$, DN represents the digital number value of each pixel R_A is the radiance additive scaling factor for the averaging Band 10

2.6. CONVERSION TO BRIGHTNESS TEMPERATURE

TOA radiance is converted to brightness temperature $BT^\circ C$ using the formula:

$$T_b = \frac{K_2}{\in\left(\frac{K_1}{A_\lambda}+1\right)} - 273.15, \tag{2}$$

where T_b is the brightness Temperature in $(^\circ C)$, K_1 and K_2 are brightness temperature constants, and A_λ is the TOA radiance.

2.7. NORMALIZED DIFFERENCE VEGETATION INDEX (NDVI) MAP

The land surface emissivity was determined using the Normalized Difference Vegetation Index (NDVI), which differentiates vegetated areas from non-vegetated ones. NDVI was calculated using data from the red (Band 4) and near-infrared (Band 5) bands

$$NDVI = \frac{B5(NIR) - B4(Red)}{B5(NIR) + B4(Red)}. \tag{3}$$

2.8. PROPORTION OF VEGETATION

The proportion of vegetation was calculated using the NDVI values according to the following formula:

$$V_p = (NDVI - NDVI_{\min}/NDVI_{\max} - NDVI_{\min})^2, \tag{4}$$

where $NDVI$ is Normalized Difference Vegetation Index, $NDVI_{\min}$ is minimum $NDVI$ value, and $NDVI_{\max}$ is maximum $NDVI$ value.

2.9. SURFACE EMISSIVITY (ε) CALCULATION

Surface emissivity (ε) was estimated based on vegetation proportions derived from land cover characteristics using the formula:

$$\varepsilon = 0.004 \times P_v + 0.986, \tag{5}$$

where P_v is the proportion of vegetation in the study area.

2.10. LAND SURFACE TEMPERATURE CALCULATION

The final LST values were computed using the emissivity-corrected brightness temperature and Planck's radiative transfer principles. This approach incorporated the central wavelengths of Bands 10 and Planck's constant to ensure precise temperature estimation. The formula is:

$$T_s = \frac{T_b}{1 + \left(\frac{\lambda . BT}{\rho}\right) . \in(\varepsilon)}, \tag{6}$$

where T_b is the brightness temperature in $(^\circ C)$, λ is the central wavelength of Band 10 (10.895 μm), ρ is the Planck's constant divided by the Boltzmann constant (14380), and ε is the calculated land surface emissivity.

3. MACHINE LEARNING MODELS FOR SURFACE TEMPERATURE (T_S) PREDICTION

3.1. ENSEMBLE LEARNING FOR SURFACE TEMPERATURE (T_S) REGRESSION

This study utilized ensemble learning methods, including Random Forest [9] K-Nearest Neighbors (KNN) [14], and XGBoost, to analyze the relationship between landsat 9 and SRTM DEM spectral data in predicting Surface Temperature. Spectral data of these imageries were used as predictors independent variables, while surface temperature data was the dependent variable. A stacking ensemble approach combined the outputs of RF, KNN, and XGBoost, leveraging their complementary strengths to produce robust and accurate surface temperature (T_s) predictions while capturing spatial variability.

3.2. RANDOM FOREST (RF)

Random Forest (RF) is a robust ensemble learning technique that improves prediction accuracy by generating multiple decision trees during the training process and aggregating their results [9]. For regression tasks, RF computes the average of the predictions generated by each tree, a process that not only improves overall accuracy but also reduces the risk of overfitting, thereby enhancing the model's generalizability (Cortes & Vapnik, 1995). RF regression was adopted in this study to predict Land Surface Temperature (LST). Notably, several researchers have employed RF for LST regression tasks with remarkable success, achieving superior performance [3, 9, 13, 19, 22]. The implementation of RF facilitates a nuanced understanding of the underlying data patterns, ultimately contributing to more reliable LST predictions for the towns under scrutiny.

$$\widehat{y} = \frac{1}{N}\sum_{i=1}^{N} f_i(x), \tag{7}$$

where $f_i(x)$ represents the prediction of the i^{th} tree, and N is the total number of trees in the forest.

3.3. K-NEAREST NEIGHBORS (KNN)

KNN is a simple yet effective algorithm that predicts the label of a sample by evaluating the majority label of its K-nearest neighbors in feature space. Its merit lies in its non-parametric nature, which makes it flexible for handling complex datasets without assuming underlying data distributions. Several authors have employed K-Nearest Neighbors (KNN) for surface temperature prediction [12, 23]. This simplicity and adaptability have rendered KNN a valuable tool for surface temperature prediction in various geospatial and environmental applications.

$$\widehat{y} = \frac{1}{k}\sum_{i=1}^{k} y_i, \tag{8}$$

where y_i is the value of the nearest neighbor.

3.4. EXTREME GRADIENT BOOSTING (XGBOOST)

The eXtreme Gradient Boosting (XGBoost) algorithm, known for its scalability and precision, was applied to predict Land Surface Temperature (LST). As an ensemble model, XGBoost builds decision trees sequentially, enhancing predictive accuracy and reducing overfitting through regularization. Several

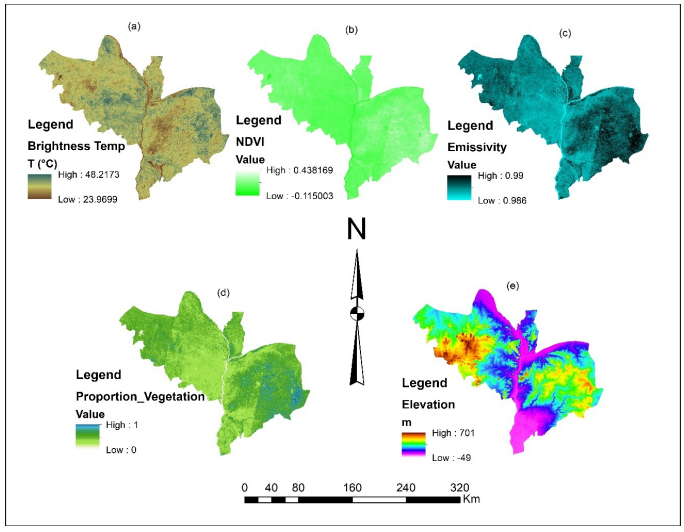

Figure 3. Brightness temperature (T_b) map, (b) Natural difference vegetation index map (c) land surface emissivity map (ε) map (d) Proportion of vegetation map (P_v) map (e) Elevation map.

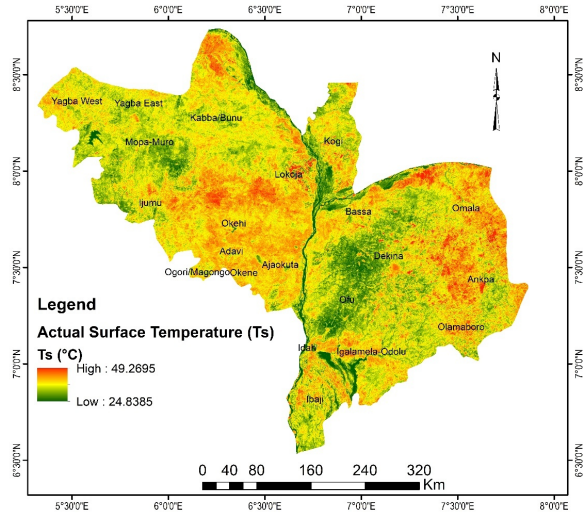

Figure 4. Surface temperature map.

researchers have successfully employed XGBoost for LST prediction [13, 22, 24, 25]. This study implemented XGBoost using Python's XGBoost library, with computations performed in Google Colab.

3.5. STACKING ENSEMBLE MODEL (SEM)

Following regression on each of the base models, a stacking ensemble model (SEM) was employed to integrate the predictions of RF, KNN, and XGBoost. This approach assigned weighted contributions to each algorithm based on their performance metrics, with a meta-learner trained on RF, KNN, and XGBoost outputs to produce the final LST predictions. By leveraging the complementary strengths of these models, SEM enhanced predictive accuracy, robustness, and generalization. Similar approaches to SEM for machine learning have been successfully utilized in previous studies [14, 26].

4. RESULTS

4.1. PREDICTOR MAPS

Figure 3 provides spatial representations of critical predictor maps derived from Landsat 9 and SRTM DEM data, which form the basis for surface temperature predictions.

4.1.1. Brightness temperature (Tb) map

Figure 3(a) illustrates the Brightness Temperature (Tb) map, obtained from the thermal infrared band 10 of Landsat 9. The map captures spatial variations in emitted thermal energy across the study area, with Tb values ranging from 23.97°C to 48.22°C. Notable patterns include urban heat islands exhibiting higher temperatures and cooler zones associated with dense vegetation

4.1.2. Natural difference vegetation index (NDVI) map

Figure 3(b) presents the Normalized Difference Vegetation Index (NDVI) map, with values spanning from - 0.115 to 0.438. High NDVI values, predominantly in forested or less urbanized zones, indicate dense vegetation, while low values highlight sparse vegetation or urbanized areas. This distribution underscores vegetation's moderating influence on surface temperature.

4.1.3. Land surface emissivity (ε) map

Figure 3(c) displays the Surface Emissivity map, with values ranging from 0.986 to 0.99. High emissivity values, typically in vegetated areas, indicate efficient thermal radiation emission, which lowers surface temperatures. Conversely, urbanized or barren areas with lower LSE values exhibit reduced emissivity, leading to heat retention. Accurate emissivity mapping is critical for refining surface temperature calculations due to the direct influence of emissivity on thermal radiation.

4.1.4. Proportion of vegetation map

Figure 3(d) illustrates the Proportion of Vegetation (P_v) map, where values range from 0 to 1. High Pv values represent dense vegetative cover, while low values denote minimal vegetation. This map identifies zones susceptible to thermal stress and vegetation loss, emphasizing the inverse relationship between vegetation density and surface temperature.

4.1.5. Elevation map

Figure 3(e) displays the elevation map of the study area, with topographic values ranging from - 49 m to 701 m. Regions with negative elevation values represent depressions, which predominantly correspond to riverine areas.

4.2. ACTUAL SURFACE TEMPERATURE (T_S) MAP

The predictor maps shown in Figure 3(a),(b),(c),(d) and (e) were integrated using GEE to generate the actual surface temperature map presented in Figure 4. The surface temperature values, ranging from 24.84°C to 49.27°C, demonstrate notable spatial variations. This map offers essential insights into the thermal properties of the area.

4.3. STACKING ENSEMBLE MODEL FRAMEWORK

Figure 5 illustrates the SEM framework obtained from integrating the derived spectral maps in Figure 3. NDVI, Pv, ε, Ts, and

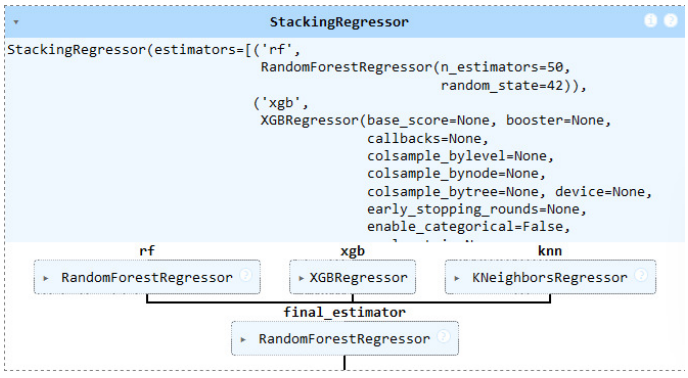

Figure 5. SEM regression framework.

elevation were used as independent variables, while the actual surface temperature spectral data served as the dependent variable for the base models. The models were individually trained using 5-fold cross-validation. The dataset was divided into five subsets, with the model trained on four subsets (80%) and tested on the remaining one (20%). This process was iterated to ensure a robust performance evaluation.

The predictions from each base model were then weighted within the SEM framework to generate the final output. The framework demonstrates how the base models: Random Forest Regressor (RF), eXtreme Gradient Boosting Regressor (XGB), and K-Nearest Neighbors Regressor (KNN) were executed. The outputs of the base models were combined using a meta-learner, implemented as a Random Forest Regressor, to produce the final predictions.

The Random Forest Regressor employed 50 decision trees (n_estimators=50) and a fixed random state (random_state=42) for reproducibility. The eXtreme Gradient Boosting Regressor, known for advanced tree-based learning and scalability, included features such as early stopping. KNN, a non-parametric model, captured localized spatial patterns. The stacking ensemble framework optimized model weights by assigning importance to each base model's prediction using the meta-learner, a Random Forest Regressor. The meta-learner leveraged feature importance and decision trees to adjust model contributions based on their predictive performance. The 5-fold cross-validation strategy ensured model robustness by systematically splitting the dataset into five subsets, with four used for training (80%) and one for testing (20%), preventing overfitting and improving generalizability. The SEM significantly enhanced predictive accuracy, outperforming the best-performing base model, RF, by 3.31% (R^2: 0.9986 vs. 0.9655), demonstrating the advantage of the ensemble approach in refining LST predictions.

The SEM aggregates predictions from the base models, leveraging their complementary strengths. Random Forest excels in handling non-linear interactions and is robust enough to overfit. XGB offers precision in high-dimensional datasets, and KNN effectively captures local spatial relationships. This hierarchical approach ensures robust and accurate predictions.

Figure 6 presents the predicted surface temperatures of the study area as derived from the meta-model, SEM. The surface temperatures are classified into three classes: high, medium, and low. This classification provides a clear spatial representation of temperature variations, aiding in the mapping of potential geothermal hotspots in Figure 7.

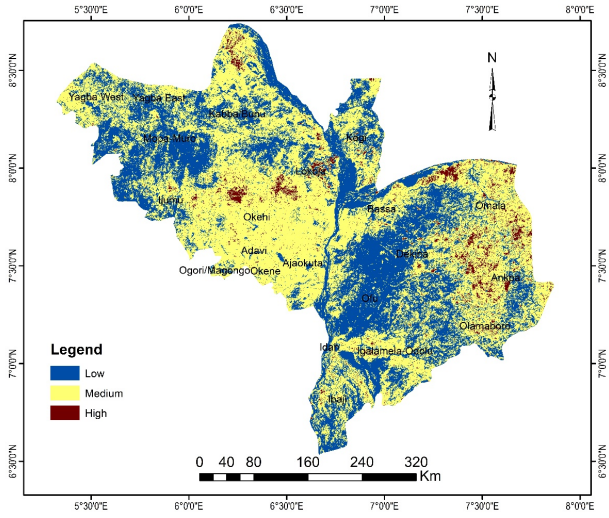

Figure 6. Predicted surface temperature map of the study.

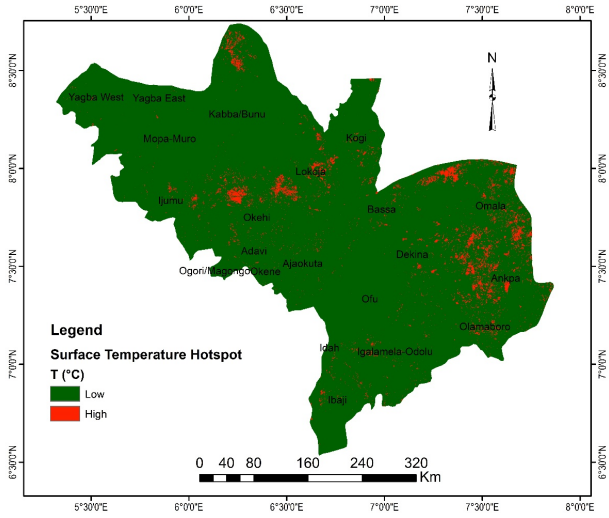

Figure 7. Surface temperature hotspot map.

The stacking ensemble framework optimized model weights through a meta-learner, specifically a Random Forest Regressor, which assigned weights based on the predictive accuracy of each base model. The base models—RF, XGBoost, and KNN—were trained individually, and their predictions were used as inputs for the meta-learner. The training process involved a 5-fold cross-validation strategy, where the dataset was split into five subsets, with four used for training (80%) and one for testing (20%), ensuring robustness and preventing overfitting. This iterative validation approach provided a reliable performance assessment.

Table 1 summarizes the performance metrics of the predictive models, while Figure 8 provides a bar chart visualization of the models' performance.

To quantify the improvement of the SEM framework over the best-performing base model, Table 1 demonstrates that SEM achieved an R^2 of 0.9986, which is a 3.31% improvement over RF (0.9655), an 8.03% increase over XGBoost (0.9183), and a

Table 1. Model performance metrics.

Model	MAE	MSE	R^2
RF	0.3421	0.5661	0.9655
XGBoost	0.4604	0.77	0.9183
KNN	0.5102	0.8573	0.8707
SEM	0.1257	0.1942	0.9986

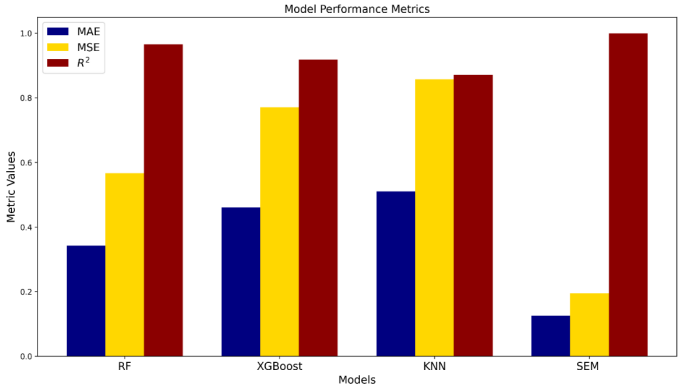

Figure 8. Bar chart showing model performance metrics.

12.79% enhancement over KNN (0.8707). Additionally, SEM reduced the Mean Absolute Error (MAE) and Mean Squared Error (MSE) significantly compared to individual models, confirming its predictive superiority. While computational efficiency was considered, Google Colab's processing capacity was sufficient for model training and execution, and no significant limitations were encountered in handling the dataset or running the SEM framework.

5. DISCUSSION

This study highlights the effectiveness of integrating Landsat 9 spectral data and SRTM DEM with machine learning for LST prediction. The SEM, combining RF, XGBoost, and KNN, achieved an R^2 of 99.86%, surpassing RF by 3.31%, XGBoost by 8.03%, and KNN by 12.79%. This supports prior studies on ensemble learning in environmental modeling [4, 13, 15]. Given its superior performance (MAE: 0.1257, MSE: 0.1942, R^2: 0.9986), hyperparameter tuning is unnecessary, as SEM effectively optimizes pixel spectral selection.

The spatial analysis of LST patterns revealed critical thermal variations influenced by vegetation cover, land surface emissivity (LSE), and elevation. Areas with high Normalized Difference Vegetation Index (NDVI) and Proportion of Vegetation (PV) exhibited lower surface temperatures due to the cooling effects of vegetation, supporting existing literature [16, 17]. Conversely, urban and barren landscapes experienced elevated temperatures due to the urban heat island (UHI) effect [6]. This confirms the need for sustainable urban planning and vegetation conservation to mitigate excessive thermal loads.

Potential biases in spectral indices can impact Land Surface Temperature (LST) predictions, particularly in regions with varying vegetation and land cover conditions. For instance, the Normalized Difference Vegetation Index (NDVI), commonly used to estimate emissivity, has limitations in arid and semi-arid regions where sparse vegetation and exposed soil can lead to overestimated or underestimated LST values [27] NDVI-based emissivity models assume a strong vegetation cover-temperature relationship, which may not hold in barren landscapes, causing inaccuracies in temperature retrieval [28].

Similarly, other spectral indices like vegetation proportion (Pv) and emissivity (*varepsilon*) are derived from NDVI, making them susceptible to the same biases. Overestimation of vegetation cover in dry environments can lead to an underestimation of LST, while underestimation in dense vegetation areas may result in overestimated LST values. These biases can introduce uncertainty in machine learning-based LST predictions, particularly in heterogeneous landscapes.

The predictive robustness of SEM was validated by performance metrics, achieving the lowest Mean Absolute Error (MAE = 0.1257) and Mean Squared Error (MSE = 0.1942). This supports the argument that no single model is universally optimal, but an ensemble approach effectively mitigates individual model weaknesses [15]. Notably, the SEM performed exceptionally well in extreme temperature conditions, which is crucial for LST modeling and environmental impact assessments [9, 11]

The identification of high-temperature zones with a threshold above 40°C aligns with the geothermal potential criteria proposed by Ref. [18]. This finding suggests that specific areas warrant further geothermal exploration. However, geothermal viability assessments require an integrative approach, incorporating subsurface thermal and geochemical analyses to complement surface temperature observations.

These findings underscore the broader implications of LST modeling in climate change mitigation, urban adaptation strategies, and renewable energy exploration. Urban heat islands (UHIs) intensify environmental challenges, necessitating policy interventions such as afforestation, green roofing, and sustainable land-use management [7, 8]. The SEM framework's ability to capture fine-scale LST variations provides policymakers with a valuable tool for climate adaptation planning and proactive environmental management [13].

6. CONCLUSION

This study successfully applied a stacking ensemble machine learning framework to predict LST using Landsat 9 and SRTM DEM data. By integrating multiple algorithms, the SEM model achieved enhanced predictive accuracy outperformed individual models, achieving an R^2 of 99.86%, surpassing RF by 3.31%, XGBoost by 8.03%, and KNN by 12.79% and capturing spatial variations in surface temperature effectively. The results emphasize the significant influence of vegetation cover, emissivity, and elevation on LST distribution, reinforcing the necessity of sustainable land-use practices in mitigating urban heat effects and climate change impacts.

The study identified high-temperature zones with geothermal potential, providing a foundational basis for targeted renewable energy exploration. However, further geophysical and geochemical investigations are required to assess the feasibility of geothermal resource exploitation. The findings also demonstrate the transformative potential of machine learning in environmental monitoring, offering a scalable and data-driven approach for climate adaptation and sustainable resource management.

Scaling SEM to larger datasets presents challenges, includ-

ing high computational costs, memory limitations, and extended training times due to multiple model executions and cross-validation. Large-scale spectral data may exceed local processing capacities, requiring cloud-based solutions. While hyperparameter tuning was unnecessary in this study, larger datasets may demand optimization to prevent overfitting. Additionally, integrating multi-source data across vast regions can be bandwidth-intensive, especially when transferring outputs between platforms like GEE and Colab. Addressing these issues requires distributed processing, cloud computing, and optimized machine learning frameworks.

The proposed SEM framework contributes to advancing LST prediction methodologies, aligning with the growing demand for interdisciplinary approaches in environmental science, renewable energy exploration, and climate resilience planning. Future research should explore the integration of deep learning models and additional environmental predictors to further enhance predictive accuracy and expand the applicability of the framework across diverse geographic and climatic conditions.

RECOMMENDATIONS

Based on the findings, the following recommendations are proposed:

1. Thermal anomalies in urban areas were innovatively detected using ensemble learning with Landsat 9 TIR Band 10. While ground truth validation was not conducted in this study, the findings establish a basis for future research to validate and expand on these results.
2. Urban and Environmental Planning: Policymakers should prioritize urban greening, afforestation, and the adoption of reflective surfaces to mitigate the UHI effect and enhance urban resilience.
3. Geothermal Energy Exploration: Identified high-temperature zones should be further investigated using geophysical techniques such as magnetotellurics and resistivity surveys to assess geothermal resource viability.
4. Advancing Machine Learning Models: Future research should integrate deep learning architectures, such as Convolutional Neural Networks (CNN) and Long Short-Term Memory (LSTM) networks, to enhance the predictive capability of LST models (Xu & Wu, 2023a, 2023b).
5. Incorporation of Additional Predictors: Further studies should incorporate environmental variables such as soil moisture, land cover classification, and atmospheric parameters to improve model performance.
6. Scalability and Validation: The SEM framework should be tested in diverse climatic and geological settings to evaluate its generalizability and computational efficiency for large-scale environmental modeling.
7. Climate Adaptation Strategies: Environmental agencies should leverage SEM-based predictions to develop targeted interventions for heatwave-prone regions, improving climate resilience and reducing thermal stress.

By addressing these recommendations, future research can build on the current findings to enhance predictive modeling, support sustainable energy resource management, and contribute to climate change mitigation efforts.

DATA AVAILABILITY

The datasets generated and analyzed during the current study are available from the corresponding author upon reasonable request. Additionally, the code used in this study has been archived in the Google Earth Engine Repository and can be accessed via the following link: https://code.earthengine.google.com/314e5d2e21134094e0d5ea649448e93e.

References

[1] M. G. Ayuba & M. K. Lawal, ''Investigating geothermal energy resource potential in parts of southwestern Nigeria using aeromagnetic data'', Science World Journal **14** (2019) 1. http://www.scienceworldjournal.org.

[2] T. Suleiman, F. N. Okeke & N. D. Obiora, ''Spectral analysis of high-resolution aeromagnetic data for geothermal energy reconnaissance across Sokoto Basin, Northwest, Nigeria'', Journal of the Earth and Space Physics **46** (2020) 147. https://doi.org/10.22059/jesphys.2020.299866.1007205.

[3] X. Zhang, Q. Zhang, G. Zhang, Z. Nie, Z. Gui & H. Que, ''A novel hybrid data-driven model for daily land surface temperature forecasting using long short-term memory neural network based on ensemble empirical mode decomposition'', International Journal of Environmental Research and Public Health **15** (2018) 1032. https://doi.org/10.3390/ijerph15051032.

[4] S. L. Ermida, P. Soares, V. Mantas, F. M. Göttsche & I. F. Trigo, ''Google earth engine open-source code for land surface temperature estimation from the landsat series'', Remote sensing (Basel) **12** (2020) 1471. https://doi.org/10.3390/RS12091471.

[5] J. Alzubi, A. Nayyar & A. Kumar, ''Machine learning from theory to algorithms: an overview'', Journal of Physics: Conference Series **1142** (2018) 012012 https://doi.org/10.1088/1742-6596/1142/1/012012.

[6] M. O. Ibitoye, O. G. Aderibigbe, S. A. Adegboyega & A. O. Adebola, ''Spatio-temporal analysis of land surface temperature variations in the rapidly developing Akure and its environs, southwestern Nigeria using Landsat data'', Ethiopian Journal of Environmental Studies and Management **10** (2017) 389. https://doi.org/10.4314/ejesm.v10i3.9.

[7] D. Dissanayake, T. Morimoto, Y. Murayama, M. Ranagalage & H. H. Handayani, ''Impact of urban surface characteristics and socio-economic variables on the spatial variation of land surface temperature in Lagos City, Nigeria'', Sustainability **11** (2019) 25. https://doi.org/10.3390/su11010025.

[8] P. Nwilo, D. Olayinka, J. Obiefuna, A. Atagbaza & A. Adzandeh, ''Determination of land surface temperature (lst) and potential urban heat island effect in parts of Lagos state using satellite imageries'', FUTY Journal of the Environment **7** (2012) 1. https://doi.org/10.4314/fje.v7i1.2.

[9] X. Wang, L. Zhong & Y. Ma, ''Estimation of 30 m land surface temperatures over the entire Tibetan Plateau based on Landsat-7 ETM+ data and machine learning methods'', International Journal of Digital Earth **15** (2022) 1038. https://doi.org/10.1080/17538947.2022.2088873.

[10] M. ID, ''Simulation and prediction of land surface temperature (lst) dynamics within Ikom city in Nigeria using artificial neural network (ANN)'', Journal of Remote Sensing & GIS **5** (2015) 1. http://dx.doi.org/10.4172/2469-4134.1000158

[11] E. K. Mustafa, ''Study for predicting land surface temperature (LST) using Landsat data: a comparison of four algorithms'', Advances in Civil Engineering **2020** (2020) 7363546. https://doi.org/10.1155/2020/7363546.

[12] K. S. Kumar, K. P. Kumari & P. U. Bhaskar, ''Artificial neural network model for prediction of land surface temperature from land use/cover images'', International Journal of Advanced Trends in Computer Science and Engineering **2** (2013) 87. https://doi.org/10.1016/p.rdf.2013.02.003.

[13] M. Witjes, L. Parente & C. J. van Diemen, ''A spatiotemporal ensemble machine learning framework for generating land use / land cover time-series maps for Europe (2000 – 2019) based on LUCAS, CORINE and GLAD Landsat'', 2022. [Online]. https://doi.org/10.21203/rs.3.rs-561383/v4.

[14] X. Xu & Y. Wu, ''Application of tree based enhanced stacking ensemble learning'', 2023. [Online]. https://doi.org/10.21203/rs.3.rs-2471395/v1.

[15] E. J. M. Carranza, ''Analysis and mapping of geochemical anomalies using logratio-transformed stream sediment data with censored values'', Journal of Geochemical Exploration **110** (2011) 167. https://doi.org/10.1016/j.gexplo.2011.05.007.

[16] O. O. Ifatimehin, ''An assessment of urban heat island of Lokoja town and surroundings using Landsat ETM data'', FUTY Journal of the Environment **2** (2007) 1. http://dx.doi.org/10.4314/fje.v2i1.50790.

[17] P. Nwaerema, O. N. Vincent, C. Amadou & A. I. Morrison, ''Spatial assessment of land surface temperature and emissivity in the tropical littoral city

of Port Harcourt, Nigeria'', International Journal of Environment and Climate Change **9** (2019) 88. https://doi.org/10.9734/ijecc/2019/v9i230099.

[18] J. Finger & D. Blankenship, ''Sandia report handbook of best practices for geothermal drilling'', 2010. [Online]. https://www1.eere.energy.gov/geothermal/pdfs/drillinghandbook.pdf.

[19] T. G. Farr *et al*., ''The shuttle radar topography mission'', Reviews of Geophysics **45** (2007) RG2004. https://doi.org/10.1029/2005RG000183.

[20] X. Ye, R. Liu, J. Hui & J. Zhu, ''Land surface temperature estimation from landsat-9 thermal infrared data using ensemble learning method considering the physical radiance transfer process'', Land **12** (2023) 1287. https://doi.org/10.3390/land12071287.

[21] USGS, ''Landsat 8-9 Calibration and Validation Algorithm Description Document'', 2021. [Online]. https://www.usgs.gov/media/files/landsat-8-9-calibration-validation-algorithm-description-document.

[22] L. Zhao, S. Lu & D. Qi, ''Improvement of maximum air temperature forecasts using a stacking ensemble technique'', Atmosphere **14** (2023) 600. https://doi.org/10.3390/atmos14030600.

[23] Astisiasari, D. R. Hizbaron & M. A. Setiawan, ''Estimation of land surface temperature in dieng volcanic complex using TIR-based satellite imageries'', IOP Conference Series: Earth and Environmental Science **451** (2020) 012066. https://doi.org/10.1088/1755-1315/451/1/012066.

[24] N. Zhang & K. Zhou, ''Mineral prospectivity mapping with weights of evidence and fuzzy logic methods'', Journal of Intelligent and Fuzzy Systems **29** (2015) 2639. https://doi.org/10.3233/IFS-151967.

[25] E. Boucher & F. Aires, ''Improving remote sensing of extreme events with machine learning: land surface temperature retrievals from IASI observations'', Environmental Research Letters **18** (2023) 024025. https://doi.org/10.1088/1748-9326/acb3e3.

[26] S. L. Ermida, P. Soares, V. Mantas, F. M. Göttsche & I. F. Trigo, ''Google earth engine open-source code for land surface temperature estimation from the Landsat series'', Remote Sensing **12** (2020) 1471. https://doi.org/10.3390/RS12091471.

[27] J. A. Sobrino, J. C. Jiménez-Muñoz & L. Paolini, ''Land surface temperature retrieval from LANDSAT TM 5'', Remote Sensing of Environment **90** (2004) 434. https://doi.org/10.1016/j.rse.2004.02.003.

[28] B. H. Tang, K. Shao, Z. L. Li, H. Wu & R. Tang, ''An improved NDVI-based threshold method for estimating land surface emissivity using MODIS satellite data'', International Journal of Remote Sensing **36** (2015) 4864. https://doi.org/10.1080/01431161.2015.1040132.